Results and Discussion

1. Raw IMS Vibration Signal

Loaded signal length: 81920 samples

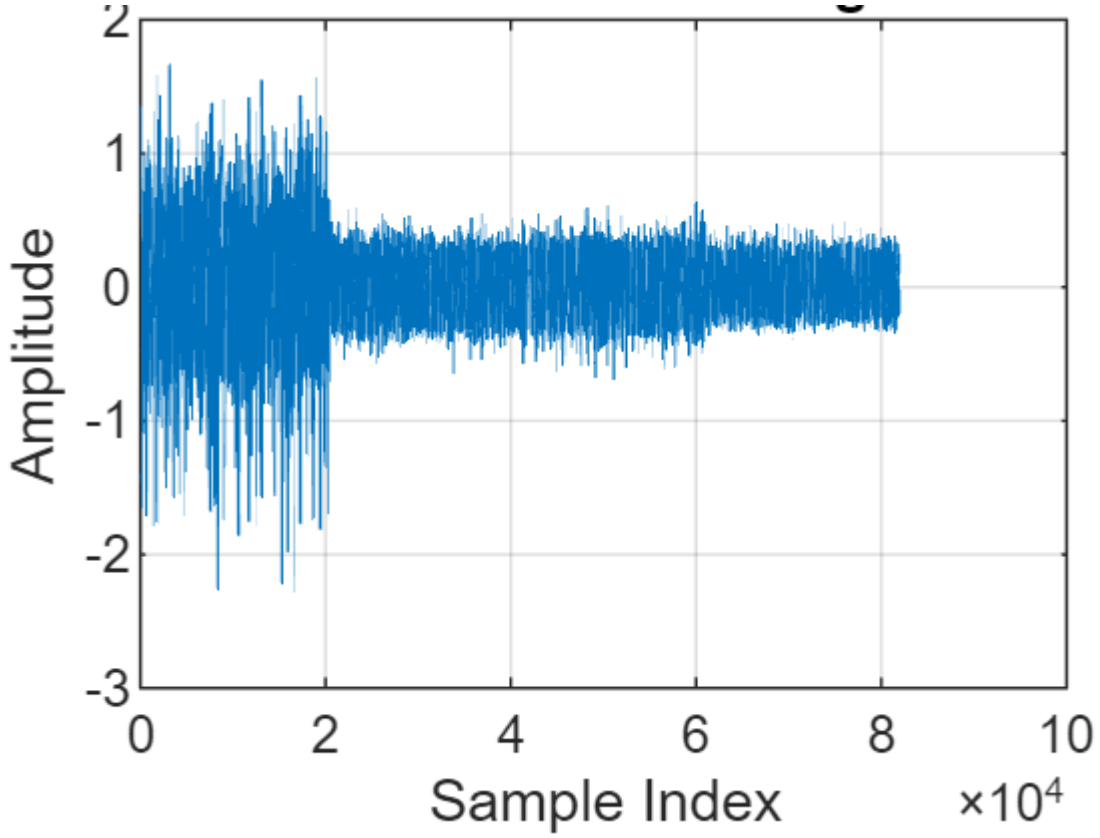

The raw IMS vibration signal exhibits strong non-stationary behaviour and is heavily dominated by broadband noise, particularly in the initial segment where large random fluctuations are observed. No clear periodic impulsive patterns associated with bearing faults are visible in the time domain, indicating that fault-related information, if present, is weak and masked by noise. The amplitude variations alone do not provide reliable diagnostic insight, highlighting the limitation of direct time-domain inspection. This motivates the need for structured matrix-based denoising to suppress noise while preserving hidden fault-induced impulses.

2. Pre-processed Signal (1 Second)

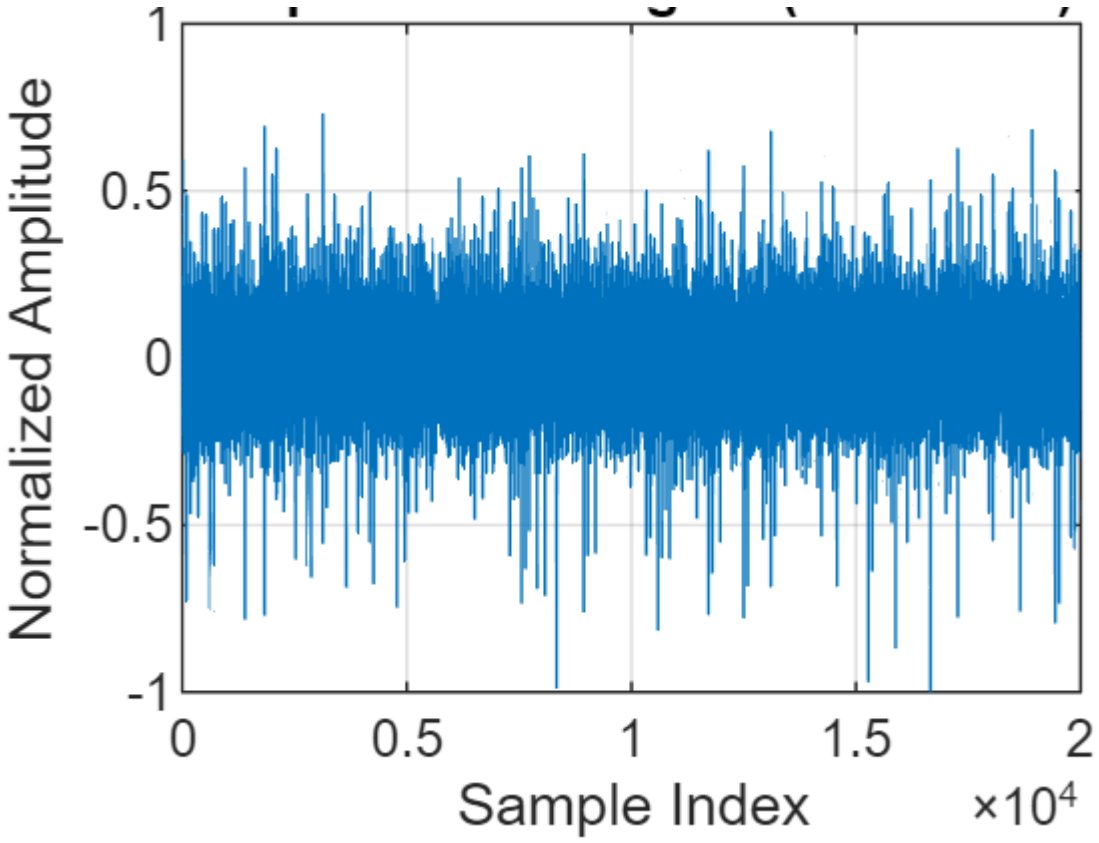

The figure shows a one-second segment of the vibration signal after preprocessing, including mean removal and amplitude normalization. These operations suppress DC bias and scale the signal to a uniform amplitude range while preserving transient and impulsive characteristics. Although the signal remains noise-dominated, the normalization ensures numerical stability and consistent energy representation for subsequent matrix construction. This preprocessing step is essential for reliable Hankel matrix formation and fair comparison across different SVD-based denoising methods.

3. Constructed Hankel Matrix

Constructed matrix size: 40 x 19961

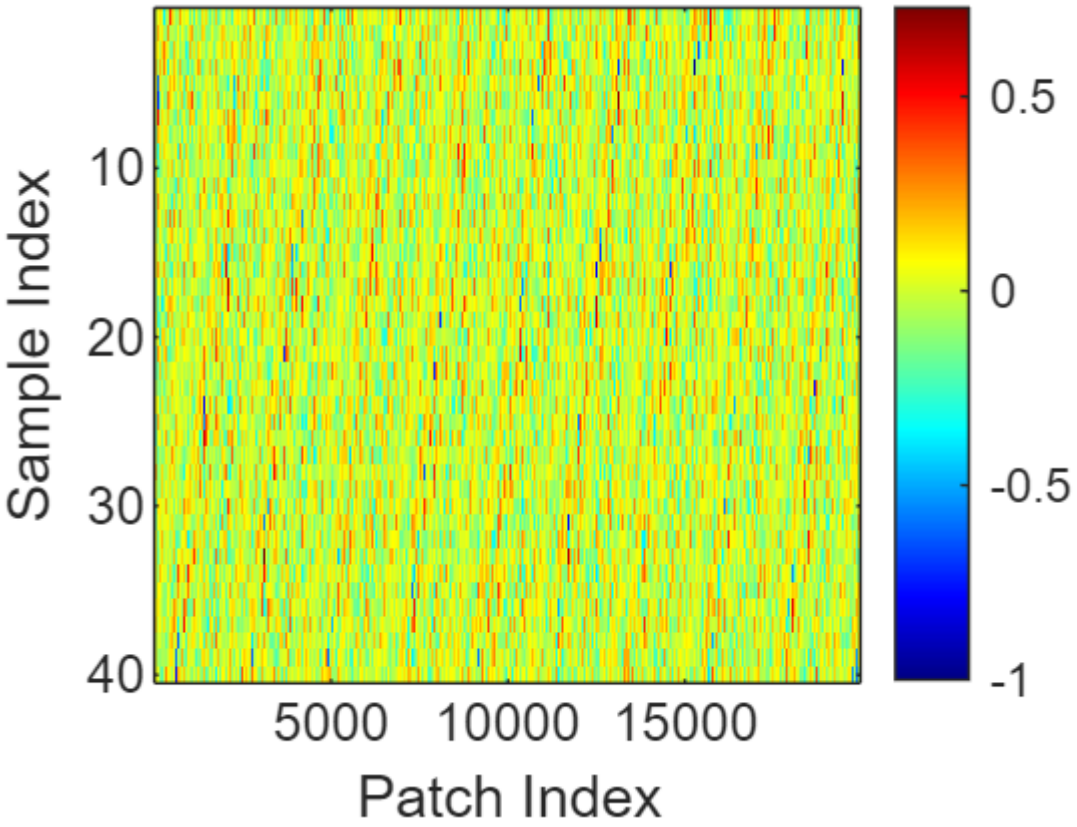

This figure visualizes the Hankel matrix constructed from the pre-processed vibration signal using a fixed window length with maximum overlap. Each column represents a shifted segment of the time-domain signal, while each row corresponds to a specific lagged sample, resulting in a structured matrix that preserves temporal correlations. The visible vertical texture indicates strong local similarity across adjacent columns, reflecting the repetitive and correlated nature of the underlying signal. This structured representation is fundamental for exploiting the low-rank property of vibration signals and enables effective separation of fault-related components and noise through Singular Value Decomposition.

4. Singular Value Distribution

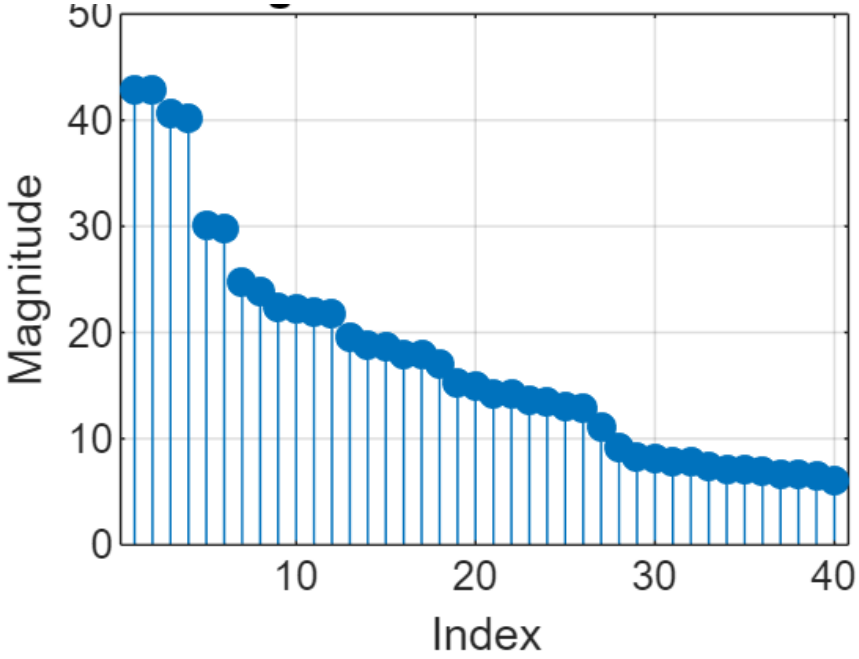

This figure shows the singular value distribution obtained from the SVD of the constructed Hankel matrix. A clear and rapid decay of singular values is observed, indicating that a small number of dominant singular components capture most of the signal's structured energy, while the remaining components primarily represent noise. This energy concentration confirms the low-rank nature of the vibration signal embedded in the Hankel matrix. The distribution directly motivates the use of SVD-based denoising methods to suppress noise while preserving fault-related information.

5. Quantitative Comparison of Denoising Performance Using Relative Reconstruction Error

```
TSVD  Error: 0.5220
RSVD  Error: 0.4654
WSSVD Error: 0.0094
```

The relative reconstruction error provides an objective measure of denoising performance. TSVD shows the highest error (0.5220), indicating significant information loss due to hard singular value truncation. RSVD improves reconstruction accuracy (0.4654) by incorporating fault-related weighting, but still suffers from amplitude distortion. In contrast, WSSVD achieves a substantially lower error (0.0094), demonstrating effective noise suppression while preserving the original signal structure. This quantitative result confirms the theoretical advantage of WSSVD as a balanced, optimization-based denoising method.

6. Time-Domain Denoising Comparison

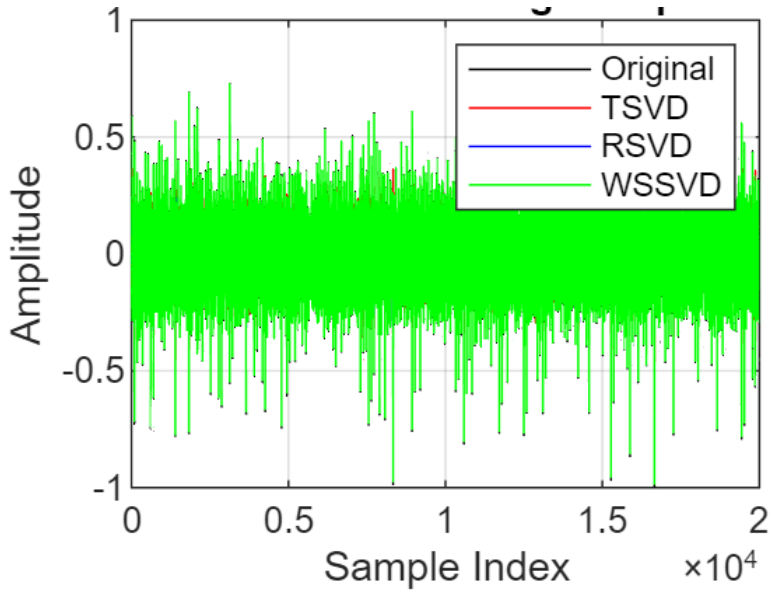

This figure compares the time-domain waveforms of the original signal and the signals denoised using TSVD, RSVD, and WSSVD. TSVD produces an overly smoothed signal due to hard truncation of singular values, resulting in the loss of transient impulsive information. RSVD enhances impulsive behaviour to some extent; however, the overall signal amplitude is noticeably reduced, indicating amplitude distortion caused by direct singular value reweighting. In contrast, WSSVD preserves clear impulsive structures while maintaining amplitude consistency with the original signal, demonstrating superior noise suppression without sacrificing physical signal characteristics. This comparison highlights the advantage of weighted soft-thresholding in achieving balanced denoising performance.

7. Bearing Fault Characteristic Frequencies

```
Shaft frequency (fr): 33.33 Hz
BPFO: 102.77 Hz
BPFI: 163.90 Hz
```

This table lists the theoretical fault characteristic frequencies calculated from the bearing geometry and rotational speed. The **shaft frequency (fr)** represents the rotational speed of the shaft and serves as the fundamental reference.

- The **Ball Pass Frequency of the Outer race (BPFO)** corresponds to defects on the outer race and manifests as periodic impacts when rolling elements pass the fault location.

- The **Ball Pass Frequency of the Inner race (BPFI)** represents inner race defects and typically appears with higher modulation due to relative motion between the fault and the sensor.

8. Envelope Spectrum Comparison for Different Denoising Methods

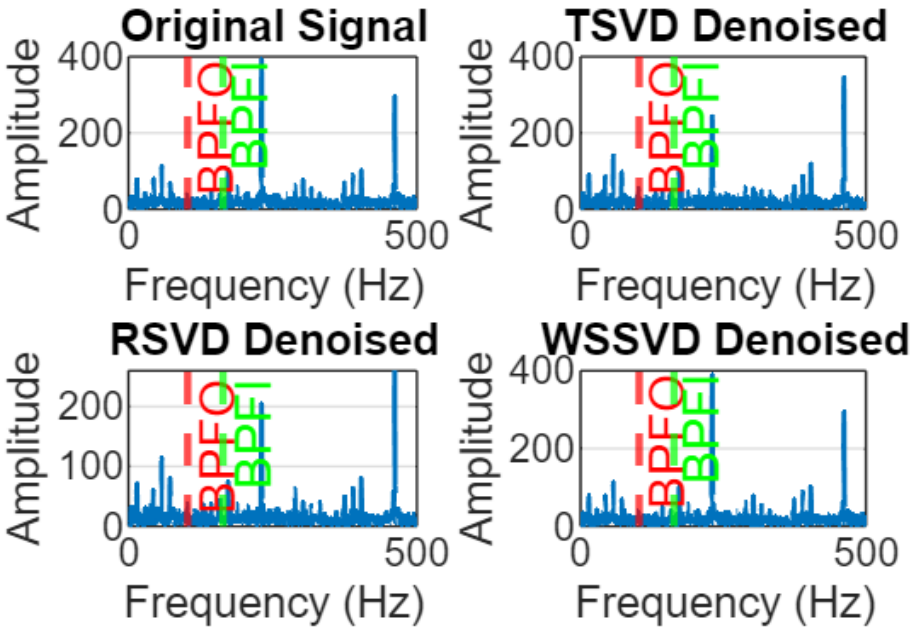

This figure compares the envelope spectra of the original signal and signals denoised using TSVD, RSVD, and WSSVD, with fault characteristic frequencies marked for reference.

- In the original signal, BPFO and BPFI components are weak and partially masked by noise, making fault identification unreliable.
- TSVD reduces background noise but fails to significantly enhance fault-related peaks due to excessive information loss.
- RSVD improves the visibility of fault frequencies; however, the amplitudes of BPFO and BPFI are

noticeably attenuated, indicating distortion caused by singular value reweighting.

- In contrast, WSSVD clearly enhances fault characteristic frequencies with higher and more stable amplitudes, demonstrating superior fault feature extraction while preserving physical signal information.

9. Extracted Impulsive Signal using WSSVD

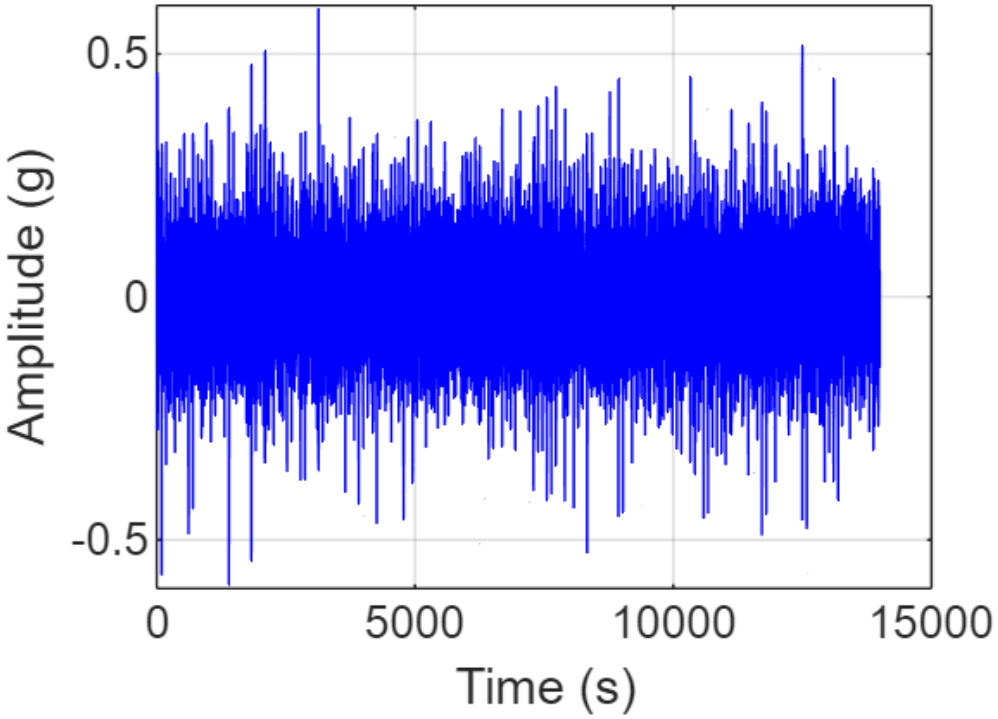

This figure shows the time-domain impulsive signal extracted after applying WSSVD-based denoising followed by resonance band filtering. Compared to the raw and conventionally denoised signals, the waveform exhibits clearer and more regularly distributed impulsive responses, indicating effective suppression of random noise and non-periodic interference. The impulsive components are preserved with consistent amplitude, reflecting the ability of

WSSVD to maintain physical signal fidelity while isolating fault-induced impacts. This result demonstrates that WSSVD successfully enhances periodic impulsive behaviour associated with bearing defects, providing a cleaner input for subsequent envelope and square envelope spectrum analysis.

10. Square Envelope Spectrum of WSSVD-Denoised Signal

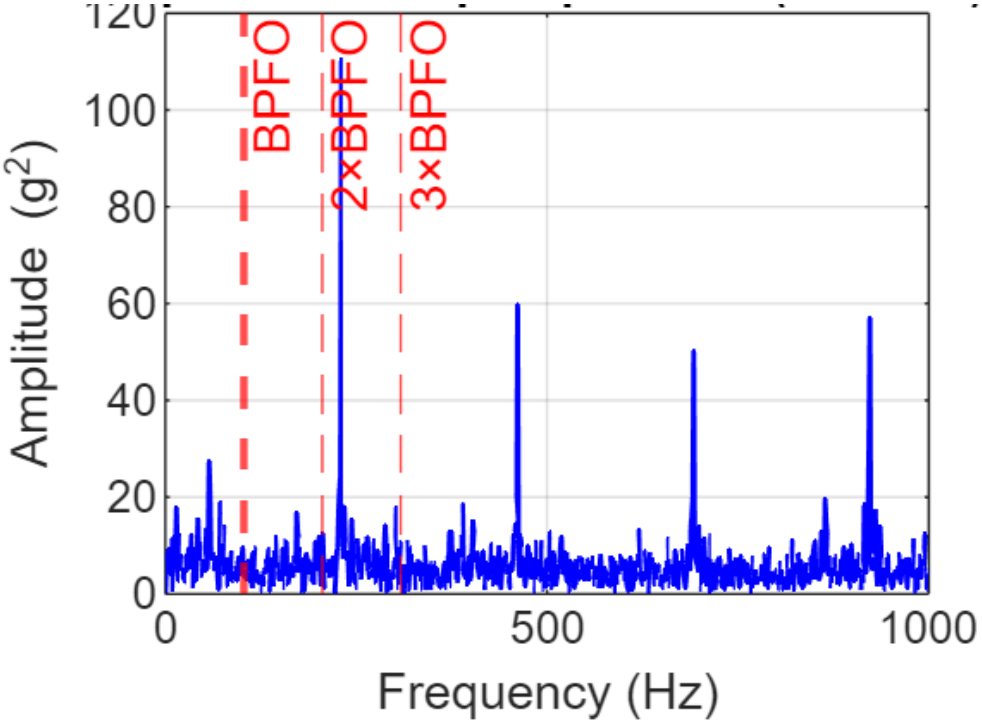

This figure presents the square envelope spectrum of the impulsive signal extracted using WSSVD, providing a clear frequency-domain representation of fault-induced periodic impacts. Distinct and prominent peaks are observed at the Ball Pass Frequency of the Outer race (BPFO) and its second and third harmonics, indicating strong periodic modulation caused by an outer race defect. The clear separation of fault-

related components from the noise floor demonstrates the effectiveness of WSSVD in suppressing random interference while preserving fault-related energy. Compared to conventional SVD-based methods, the enhanced amplitude and harmonic clarity confirm that WSSVD enables more reliable fault feature extraction and diagnosis, even under low signal-to-noise conditions.